PCCP

Cite this: *Phys. Chem. Chem. Phys.*, 2011, **13**, 14050–14063

www.rsc.org/pccp

PAPER

A combined Raman- and infrared jet study of mixed methanol–water and ethanol–water clusters†

Marija Nedić, Tobias N. Wassermann,‡ René Wugt Larsen§ and Martin A. Suhm*

Received 20th January 2011, Accepted 7th March 2011
DOI: 10.1039/c1cp20182d

The vibrational dynamics of vacuum-isolated hydrogen-bonded complexes between water and the two simplest alcohols is characterized at low temperatures by Raman and FTIR spectroscopy. Conformational preferences during adaptive aggregation, relative donor/acceptor strengths, weak secondary hydrogen bonding, tunneling processes in acceptor lone pair switching, and thermodynamic anomalies are elucidated. The ground state tunneling splitting of the methanol–water dimer is predicted to be larger than 2.5 cm^{-1}. Two types of alcohol–water trimers are identified from the spectra. It is shown that methanol and ethanol are better hydrogen bond donors than water, but even more so better hydrogen bond acceptors. As a consequence, hydrogen bond induced red shifts of OH modes behave non-linearly as a function of composition and the resulting cluster excess quantities correspond nicely to bulk excess enthalpies at room temperature. The effects of weak C–H···O hydrogen bonds are quantified in the case of mixed ethanol–water dimers.

1. Introduction

Hydrogen bonds between alcohol and water molecules are of broad interest, which ranges from fundamental questions concerning conformational and donor/acceptor preferences upon pairing to the optimization of ethanol/water separation techniques in bio-fuel production. Somewhere in between these goals, aspects of hydrogen bond cooperativity and hydrophobic effects must be addressed. They are thought to be responsible for bulk thermodynamic anomalies[1] such as heats of mixing[2,3] and volume contractions,[4,5] but they are expected to emerge already on a nanoscopic scale, at the level of hydrogen-bonded clusters.[6]

Remarkably little is known experimentally about the smallest building blocks of aqueous solutions of alcohols. Microwave spectroscopy has unravelled the structure of the methanol–water dimer,[7] but not of the ethanol–water dimer, to date. Infrared spectra of such dimers and larger clusters are only known in matrix isolation,[8] but not in vacuum isolation, which lends itself better to the direct comparison between theory and experiment. Raman spectra of isolated ethanol–water clusters have recently been obtained[9] and were shown to provide molecular insights into the exothermicity of alcohol–water mixtures. One reason for the sparsity of experimental data is the absence of a suitable UV chromophore which would allow for sensitive double-resonance spectroscopy approaches.[10] VUV double resonance techniques might be feasible, but are still in their infancy[11] and do not always provide faithful infrared spectra.[12] Therefore, the direct absorption approach is currently more practical in the infrared. Among the different techniques, FTIR spectroscopy has proven to be powerful. Its high resolution capabilities[13] are less important for these flexible and multidimensional systems, but a high-throughput low-resolution variant using synchronously pulsed expansions[14,15] has been applied successfully to a range of alcohol clusters.[6] In the Raman case, high resolution is also mostly useful for the monomer constituents,[16] whereas the cluster detection profits from a low-resolution approach using a high-power excitation laser.[17]

The lack of experimental data has not slowed down computational activities in this section of molecular cluster research. These activities are indeed numerous due to the industrial importance of the bulk mixtures. Calculations using the MP2 approximation showed that water acts as a donor in mixed methanol as well as in mixed ethanol dimers.[18,19] Molecular Dynamics (MD) simulations lead to the same conclusions.[20] Zero-point energy contributions have to be taken into account for a reliable energy sequence.[21] In the case of mixed trimers the cyclic structures were found to be more stable than linear ones at B3LYP as well as MP2 levels.[22] Differences among the energies of the mixed trimers turned

Institut für Physikalische Chemie, Universität Göttingen, Tammannstr. 6, 37077 Göttingen, Germany. E-mail: msuhm@gwdg.de
† Electronic supplementary information (ESI) available. See DOI: 10.1039/c1cp20182d
‡ Present address: Laboratoire de Chimie Physique Moléculaire, École Polytechnique Fédérale de Lausanne, Station 6, CH-1015 Lausanne, Switzerland
§ Present address: Department of Chemistry, University of Copenhagen, Universitetsparken 5, DK-2100 Copenhagen, Denmark

out to be small.[22,23] A DFT study on (methanol)$_3$–water and (ethanol)$_3$–water heterotetramers revealed that the 4-ring structure is preferred due to cooperative effects. It also showed that cooperative effects increase when each molecule simultaneously acts as a hydrogen bond donor and acceptor.[24] A detailed quantum-chemical study on small methanol–water clusters confirmed the increasing cooperative effects from trimers to tetramers.[25]

Here, we present the first FTIR spectra of vacuum-isolated small alcohol–water clusters and we provide details and extensions on recently reported[9] corresponding Raman spectra. We concentrate on the two simplest alcohols, namely methanol and ethanol. Methanol serves as a case where conformational isomerism in the monomers is absent, whereas ethanol includes this interesting degree of freedom and was also chosen for its practical importance. Jet relaxation studies[26,27] help to identify the most stable conformations. The analysis of donor/acceptor preferences rests on the formalism presented in ref. 28 and spectroscopic excess quantities in the mixing process are compared to empirical correlations between thermodynamic and spectroscopic data.[29]

Alcohol–water dimers provide valuable information on weak hydrogen bonds between C–H groups and oxygen atoms.[30] In contrast to conformational preferences in covalently bound molecules such as propanol,[31] there is much less strain imposed by the connecting O–H$\cdots$O hydrogen bond in such a dimer. Therefore, the weak C–H$\cdots$O interactions can be probed more independently. As we will see, there are indeed subtle spectral and energetic effects which correlate with the C–H$\cdots$O contact.

2. Methods

2.1 FTIR spectroscopy

The FTIR-jet spectrometer used to obtain the IR spectra has been described elsewhere.[32,33] It consists of a high-throughput slit nozzle which is fed by an array of six pulsed magnetic valves. Two temperature controlled saturators filled with pure alcohol and water are used to dope two separate flows of helium which then mix with a third stream of pure helium in a reservoir, providing helium with traces of alcohol and water (up to 0.6%). Relative concentrations are roughly estimated based on relative intensities, vapor pressures, and mixing ratios. The 135 ms gas pulses are synchronized to a rapid-scan Bruker Equinox 55 FTIR spectrometer (2 cm^{-1}, tungsten source, InSb detector, CaF_2 beam splitter, and band pass filters). Spectra from 150–200 pulses were averaged for the presented spectra. More details can be found in the supplement (Table S1, ESI†).

2.2 Raman spectroscopy

Different variants of the Raman-jet setup were used.[9,34–37] Basically, it consists of a 18 W 532 nm Nd : YVO_4 laser source focusing on a supersonic jet expansion from a 4.0 × 0.15 mm^2 slit nozzle which is fed by two streams of helium with traces (up to 1.0%) of alcohol and water (see Subsection 2.1). The jet chamber is evacuated by a 250 m^3 h^{-1} roots pump backed up by a 100 m^3 h^{-1} rotary vane pump. In the case of the methanol–water and deuterated methanol–deuterium oxide measurements, a 500 m^3 h^{-1} roots pump was added to increase the pumping capacity. The excitation laser is focused by a planoconvex lens. A McPherson Inc. Model 2051 monochromator or a McPherson 205f spectrograph disperse the scattered radiation onto a Princeton Instruments Spec-10:400B/LN CCD camera. Wavelength calibration is carried out with Ne atomic fluorescence lines. The absolute wavenumber scale is expected to be accurate within 1–2 cm^{-1}. The final spectra result from a smoothed average of four to twelve independent acquisitions with an integration time of 200–600 s. Further details are provided in the ESI† (Tables S2–S4).

2.3 Chemicals and nomenclature

Methanol (MeOH, Acros Organics, >99.5%), methanol-d1 (MeOD, Cambridge Isotope Lab., 99%), ethanol (EtOH, Merck-Suchardt resp. Carl Roth, ≥99.5%), ethanol-d1 (EtOD, Aldrich, 99%), water (H_2O, Roth Rotipuran, p.a.), deuterium oxide (D_2O, Cambridge Isotope Lab., 99.9%), helium (He, 99.996%, Air Liquide), and argon (Ar, 99.998%, Air Liquide) were used as supplied. Mixing ratios are provided as **a** : **w**, *i.e.* alcohol to water molar ratios.

Ethanol exists in a *trans* (**t**, also antiperiplanar) and in two enantiomeric *gauche* (synclinal) conformations (**g**+, **g**−), which are 0.47 kJ mol^{-1} higher in energy.[38,39] Starting with the **t** conformation and looking along the O→C bond vector in a Newman projection, **g**+ is the conformation in which the O–H bond is rotated clockwise by 120°. When ethanol engages in a hydrogen bond with water as the donor, a new asymmetric center emerges at the oxygen atom of the alcohol. In a simplistic view,[6] there is a choice between two oxygen lone pairs. Looking again along the O→C bond vector, we denote the lone pair in a clockwise direction from the O–H bond as the right lone pair[34,39] as shown in Fig. 1. In the case of enantiomeric complexes, we always discuss the one where this right lone pair is engaged in the hydrogen bond.

Both alcohol (**a**) and water (**w**) can act as proton donors and acceptors. **aw** is used to describe dimers where the alcohol is the proton donor whereas **wa** describes water in the role of the donor. In cyclic trimers the sequence of letters is irrelevant, since every molecule acts simultaneously as a donor and an acceptor. Relative to the cyclic hydrogen bond plane, molecules pointing up are indicated by *u* whereas molecules pointing down are marked by *d*.

2.4 Quantum chemical calculations

There are numerous quantum-chemical calculations for methanol, ethanol and their complexes with water available

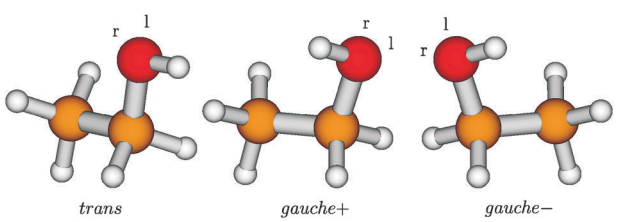

Fig. 1 Illustration of *trans*, *gauche*+, *gauche*− ethanol conformations, and the right (r) and left (l) lone pairs.

in the literature. Results for methanol–water dimers can be found in ref. 18, 19, 21, 23, 25, and 40–44, among others. Data for higher clusters are summarized in ref. 23, 24, and 42, whereas simulations on aqueous methanol mixtures were described in ref. 20 and 45. Calculations for mixed ethanol–water dimers are presented in ref. 18, 19, 41, 43, 46, and 47. Others also performed studies on higher ethanol–water clusters (*e.g.* see ref. 22, 24, and 48). In the present work, some of these calculations had to be repeated and complemented in order to obtain all information relevant for this study. For example, in ref. 18, 43, 47, and 48 conformational isomerism of ethanol was not considered. Ref. 19 and 41 distinguish between *trans* and *gauche* ethanol but do not take into account the *gauche*+ and *gauche*− variants which are spectroscopically distinguishable in mixed dimers (*vide infra*). In addition Raman intensities were rarely calculated or a given level of approximation was not available for both alcohols. To identify trends between methanol and ethanol in our work, reliable comparisons are indispensable (Tables 1 and 2). Calculations were carried out for all conceivable dimer structures (**aw** and **wa** including torsional variants). In the case of ethanol the different conformers were considered. For mixed cyclic trimers (**aaw** and **aww**) no systematic calculations on all possible conformers were carried out due to expected and experimentally confirmed spectral overlap.

The levels of calculations pursued in this work (with their abbreviations given in parentheses) include B3LYP/6-311+G(d) (B3-S), MP2/6-311+G(d) (MP2-S), MP2/6-311++G(2d,p) (MP2-M) and MP2/6-311++G(3df,2p) (MP2-L). The MP2 calculations use frozen core orbitals and all calculations were carried out using the Gaussian03 package.[49] HF calculations are largely inadequate for the investigated clusters and even fail for monomers. Note that a recent Hartree–Fock study of ethanol[50] is incorrect when claiming that its harmonic OH/OD stretching wavenumbers closely match anharmonic (solution phase) fundamentals. Indeed, they differ by about 15%.

To compensate empirically for some deficiencies in the electronic structure treatment and from other effects, the average of the corresponding harmonic OH stretching wavenumbers ω(th,n) calculated at the MP2-S and MP2-M levels was used. This *ad hoc* choice should be viewed as a pragmatic interpolation approach in the absence of more rigorous systematic calculations including larger clusters which we hope this work will trigger. Such calculations will have to address the issues of basis set superposition error in particular at the MP2 level and dispersion corrections at the density functional level. We did not use dispersion-corrected DFT in the present work, because the focus is on hydrogen bond-induced shifts. These are typically severely overestimated by gradient-corrected DFT methods in alcohol clusters.[51] However, they are expected to describe the weak C–H···O bonds better than B3LYP calculations.

The average harmonic dimer and trimer OH stretching wavenumbers ω(th,n) were shifted by the difference between the experimental water dimer donor wavenumber $\tilde{\nu}_{\mathbf{ww}}$(exp) (3602 cm^{-1} for $(H_2O)_2$ in the IR and Raman case, 2632 cm^{-1} for $(D_2O)_2$) and the corresponding harmonic wavenumber prediction $\omega_{\mathbf{ww}}$(th) (see Tables S5–S8, ESI†):

$$\tilde{\nu}(\text{th},n) = \omega(\text{th},n) + \tilde{\nu}_{\mathbf{ww}}(\text{exp}) - \omega_{\mathbf{ww}}(\text{th}) \quad (1)$$

Table 1 Experimental FTIR- and Raman-jet band positions $\tilde{\nu}$ in cm^{-1} together with proposed assignments, excess wavenumbers $\Delta_E\tilde{\nu}$ in cm^{-1}, and excess enthalpies $\Delta_E H$ in kJ mol^{-1} for pure and mixed methanol–water dimers, trimers and tetramers as well as for pure and mixed deuterated methanol–deuterium oxide dimers and trimers

Assignment	$\tilde{\nu}_{\text{FTIR}}$	$\tilde{\nu}_{\text{Raman}}$	$\Delta_E\tilde{\nu}$	$\Delta_E H$
ww	3602	3602	0	0.0
mm	3575	3577	0	0.0
wm	3567	3568	−23	−1.8
wm (shoulder)		3565.5		
www, **mmw**	3533			
mww, **mmw**	3514			
www		3491	0	0.0
mmm	3475			
mww	3439	3440	−25	−1.2
mmw		3425	−15	−0.7
mmm		3414	0	0.0
$\mathbf{w}_4$	3400[a]			
$\mathbf{w}_4$		3341[b]	0	0.0
$\mathbf{m}_4$	3294			
$\mathbf{m}_3\mathbf{w}$ (?)		3239	−5	−0.2
$\mathbf{m}_4$		3212	0	0.0
$\mathbf{w}_5$	3355[a]			
$\mathbf{w}_5$		3311[c]	0	0.0
$\mathbf{m}_4\mathbf{w}$ (?)		3191	−5	−0.2
$\mathbf{m}_5$		3167	0	0.0
mm (deuterated)		2637	0	0.0
ww (deuterated)		2632	0	0.0
wm (deuterated)		2611	−24	−1.5
www (deuterated)		2557	0	0.0
mmm (deuterated)		2530	0	0.0
mww (deuterated)		2526	−22	−1.1
mmw (deuterated)		2526	−13	−0.5

[a] See also ref. 75. [b] Average of two components at 3334 and 3347 cm^{-1}.[36] [c] Tentative assignment.[36]

Table 2 Experimental FTIR- and Raman-jet band positions $\tilde{\nu}$ in cm^{-1} together with proposed assignments, excess wavenumbers $\Delta_E\tilde{\nu}$ in cm^{-1}, and excess enthalpies $\Delta_E H$ in kJ mol^{-1} for pure and mixed ethanol–water dimers and trimers as well as for pure and mixed deuterated ethanol–deuterium oxide dimers

Assignment	$\tilde{\nu}_{\text{FTIR}}$	$\tilde{\nu}_{\text{Raman}}$	$\Delta_E\tilde{\nu}$	$\Delta_E H$
$\mathbf{we}_{t,A}$, $\mathbf{ee}_{t,A}$		3671		
ww		3602	0	0.0
$\mathbf{we}_t$		3551	−24	−2.6
$\mathbf{we}_{g+}$	3548	3548	−19	−2.3
$\mathbf{e}_g\mathbf{e}_t$	3547[a]	3548[b]	0	0.0
ee	3541	3544	0	0.0
$\mathbf{e}_{g+}\mathbf{e}_{g+}$	3531[a]	3532[b]	0	0.0
www	3531			
eew	3505			
www		3491	0	0.0
eew	3457			
eee	3449			
eww		3427	−29	−1.3
eew		3409	−12	−0.6
eee		3386	0	0.0
ww (deuterated)		2632	0	0.0
$\mathbf{e}_g\mathbf{e}_t$ (deuterated)		2621[b]	0	0.0
ee (deuterated)		2615[b]	0	0.0
$\mathbf{e}_{g+}\mathbf{e}_{g+}$ (deuterated)		2609[b]	0	0.0
$\mathbf{we}_t$ (deuterated)		2602	−25	−2.1
$\mathbf{we}_{g+}$ (deuterated)		2601	−20	−1.8

[a] Taken from ref. 39. [b] See also ref. 37.

Zero point energy corrections to binding energies were estimated in the harmonic approximation. This may not be a satisfactory approximation for the large amplitude torsions and for intermolecular degrees of freedom.[21]

IR intensities I were calculated as integrated band strengths in units of km mol^{-1}. Raman intensities depend on the wavenumber of the used laser $\tilde{\nu}_0$. Scattering cross sections σ in units of m^2 sr^{-1} can be calculated using the calculated scattering activities A_{Raman}:[37]

$$\sigma = \frac{2\pi^2 h}{45c\tilde{\nu}_k} \frac{(\tilde{\nu}_0 - \tilde{\nu}_k)^3 \tilde{\nu}_0}{1 - e^{\frac{-hc\tilde{\nu}_k}{kT}}} g_k A_{\mathrm{Raman}} \quad (2)$$

Because the investigated vibrational energies are much higher than the thermal excitation in the jet, $hc\tilde{\nu}_k \gg kT$ was assumed.

Predicted intensities were modified taking into account the approximate alcohol mole fraction $x_{\mathbf{a}}$ as well as the number of possible conformers. The probability p for a given cluster type was estimated by a binominal distribution, leading to the following equations for dimers:

$$\begin{aligned} p_{\mathbf{ww}} &= (1 - x_{\mathbf{a}})^2 \\ p_{\mathbf{wa}} &= (1 - x_{\mathbf{a}})x_{\mathbf{a}} \\ p_{\mathbf{aw}} &= x_{\mathbf{a}}(1 - x_{\mathbf{a}}) \\ p_{\mathbf{aa}} &= (x_{\mathbf{a}})^2 \end{aligned} \quad (3)$$

and trimers:

$$\begin{aligned} p_{\mathbf{www}} &= (1 - x_{\mathbf{a}})^3 \\ p_{\mathbf{aww}} &= 3x_{\mathbf{a}}(1 - x_{\mathbf{a}})^2 \\ p_{\mathbf{aaw}} &= 3(x_{\mathbf{a}})^2(1 - x_{\mathbf{a}}) \\ p_{\mathbf{aaa}} &= (x_{\mathbf{a}})^3 \end{aligned} \quad (4)$$

To account for the lower abundance of trimers relative to dimers in the supersonic expansions, empirical intensity scaling factors are applied for the simulated spectra. For the methanol–water trimers, intensity scaling factors of $\frac{1}{2}$ and $\frac{1}{4}$ are applied for the simulated Raman and IR spectra, respectively. For the ethanol–water trimers, an intensity scaling factor of $\frac{1}{4}$ is applied for both the simulated spectra. Furthermore, the average intensities predicted by the MP2-S and MP2-M levels were used for the simulated spectra (see Fig. 4, 6 and 9 later on, based on the relative intensity information σ_{rel} and I_{rel} gathered in Tables S6–S8, ESI†).

2.5 Donor/acceptor quality

When a hydrogen bond is formed between an aliphatic alcohol (**a**) and water (**w**), one molecule acts as the hydrogen bond donor and the other one as the hydrogen bond acceptor. Which role each molecule assumes depends on the relative hydrogen bond donor- and acceptor strengths as well as on subtle secondary interactions.[28] Energetic donor/acceptor scales are particularly desirable, but difficult to extract from experiment. Furthermore, they are necessarily global in nature, integrating over all interaction sites. Spectroscopic scales based on hydrogen-bond induced bathochromic shifts are more easily accessible by experiment and may provide a better representation of the local hydrogen bond environment.

The hydrogen bonded dimers **ww**, **aa**, **wa**, and **aw** involve different combinations of the alcohol monomer **a** and the water molecule **w**, where the first letter in the dimer refers to the donor and the second to the acceptor. Let **wa** be more stable than **aw** and let $D(\mathbf{wa})$ be the dissociation energy of **wa** into its fragments **w** and **a**, where conformationally diverse monomers should be taken in the closest stable conformation (*i.e.* the closest local minimum on the monomer potential surface). Thus, we have the isomeric difference ΔE_D:[28]

$$\Delta E_D = D(\mathbf{wa}) - D(\mathbf{aw}) > 0 \quad (5)$$

The donor strength of **w** relative to **a**, $D_{\mathbf{wa}}$, can be defined as:

$$D_{\mathbf{wa}} = \frac{(D(\mathbf{wa}) - D(\mathbf{aa})) + (D(\mathbf{ww}) - D(\mathbf{aw}))}{2} \quad (6)$$

It describes the average energy gain when **a** is replaced by **w** as a donor in one of the four dimers.

The corresponding acceptor strength of **w** relative to **a**, $A_{\mathbf{wa}}$, may be expressed as follows:

$$A_{\mathbf{wa}} = \frac{(D(\mathbf{ww}) - D(\mathbf{wa})) + (D(\mathbf{aw}) - D(\mathbf{aa}))}{2} \quad (7)$$

It describes the average energy gain when **a** is replaced by **w** as an acceptor in one of the four dimers.

The experimentally observable isomer difference ΔE_D is thus simply given by:

$$\Delta E_D = D_{\mathbf{wa}} - A_{\mathbf{wa}} \quad (8)$$

Accordingly, **wa** is less stable than **aw** if the relative donor strength of **w** does not reach the relative acceptor strength of **w**. $D_{\mathbf{wa}}$ and $A_{\mathbf{wa}}$ need not have opposite signs, *i.e.* the poorer donor does not have to be the better acceptor. If one changes the perspective and looks at the donor and acceptor strengths of the alcohol relative to water, all quantities change sign.

A similar analysis from a spectroscopic perspective involves the hydrogen bond-induced red shifts of X–H stretching fundamentals. For a given donor, these red shifts reflect the acceptor strength of the hydrogen bond partner, whereas the donor strength would have to be probed by less accessible acceptor vibrations. The sensitivity of hydrogen bond-induced red shifts provides an excellent spectroscopic probe of the acceptor strength, defined by donor fundamental wavenumbers $\tilde{\nu}$ according to

$$A_{\mathbf{wa}}^{\mathrm{spec}} = -\frac{(\tilde{\nu}(\mathbf{ww}) - \tilde{\nu}(\mathbf{wa})) + (\tilde{\nu}(\mathbf{aw}) - \tilde{\nu}(\mathbf{aa}))}{2} \quad (9)$$

$A_{\mathbf{wa}}^{\mathrm{spec}}$ may or may not correlate with the energetical quantity $A_{\mathbf{wa}}$ from eqn (7). The negative sign in front of the fraction results from the typical low-frequency shift of donor vibrations upon strong hydrogen bond formation.

The present analysis does not rely on the validity of energy/red shift and similar correlations.[29,52,53] However, such correlations will be explored when drawing thermodynamic conclusions in Section 3.4.

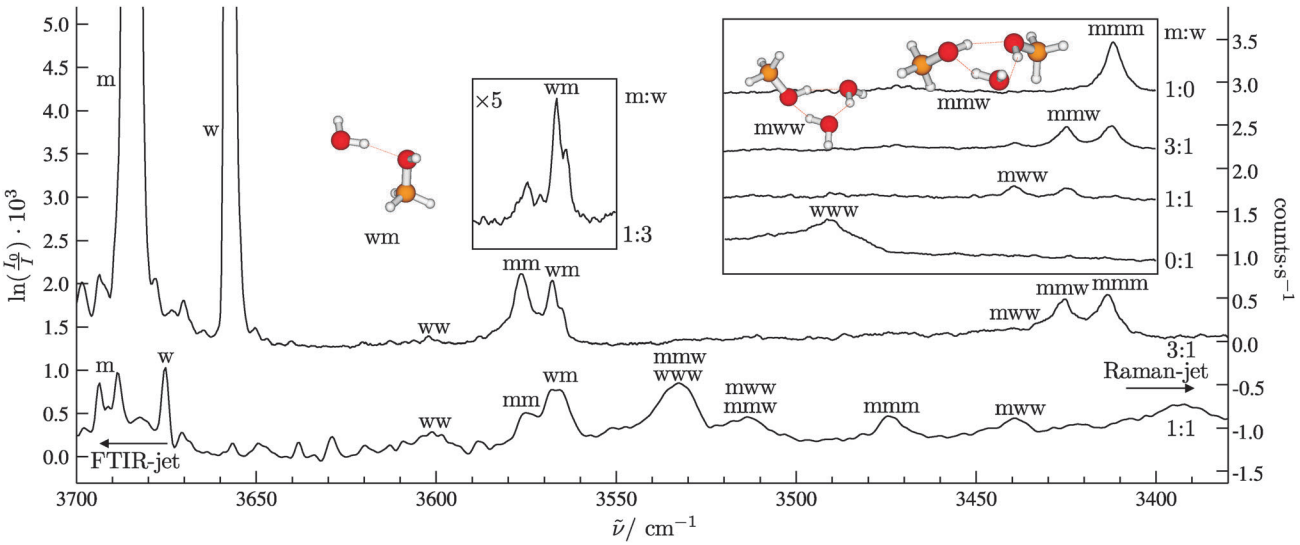

Fig. 2 Raman- and FTIR-jet spectra of the mixed methanol–water system in the OH stretching region. Absorbance magnification factors are shown in the insets, which share the wavenumber scale of the main spectra. The left inset shows the effect of reduced methanol concentration, helping in the mixed dimer assignment. The right inset shows the evolution of mixed trimers with increasing methanol-to-water ratio.

3. Results and discussion

3.1 Methanol–water

Fig. 2 provides an overview of the OH stretching region of the mixed methanol–water system by comparing Raman- and FTIR-jet spectra with assignments of the corresponding clusters. Bands appearing in spectra of the mixed system but not in the pure ones were assigned to mixed clusters. A list of assigned bands can be found in Table 1. Small IR/Raman differences of band positions are within the Raman calibration accuracy.

The mixed band near 3567 cm^{-1} appears in Raman- and FTIR-jet spectra, consistent with a dimer origin. It corresponds to the band at 3508 cm^{-1} observed in size selected ternary benzene–methanol–water trimers.[10] Two dimers **mw** and **wm** are found at all levels of calculation (see Fig. 3). For a better comparison between experimental and calculated spectra the harmonic predictions of both dimers (see Tables S9–S11, ESI†) are shown in Fig. 4. At the top the experimental Raman-jet spectrum and at the bottom the experimental FTIR-jet spectrum from Fig. 2 is repeated. In between, relative Raman scattering powers σ_{rel} and IR band strengths I_{rel} of mixed and pure clusters are plotted as stick spectra (for the scaling procedures see Section 2.4). The OH stretching band of **mw** is predicted at a higher wavenumber than **ww** where no

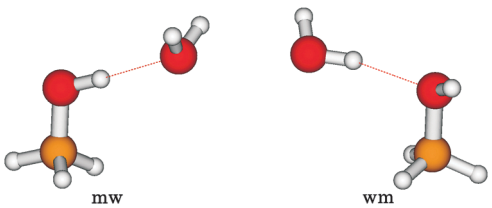

Fig. 3 Structures of the **mw** and **wm** dimer configurations at the MP2-L level.

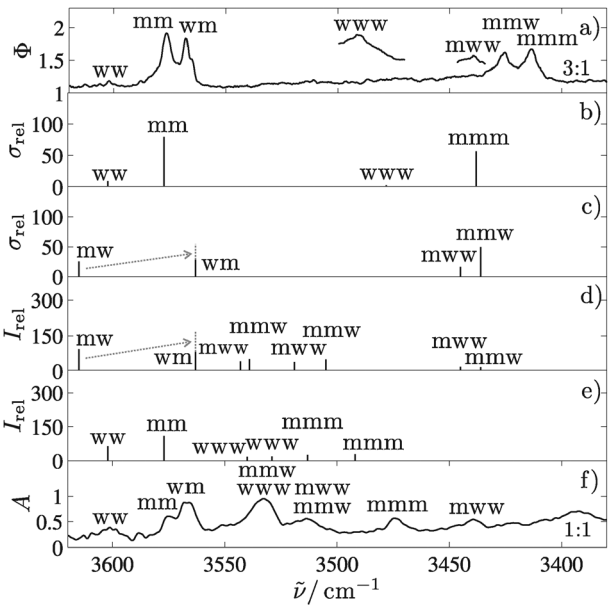

Fig. 4 Comparison of calculated (MP2-S/MP2-M average) and experimental Raman and FTIR spectra of pure and mixed dimers and trimers of the methanol–water system: (a) Raman-jet (Φ in s^{-1}), (b) Raman prediction for pure clusters (σ_{rel} in 10^{-36} m^2 sr^{-1}), (c) Raman prediction for mixed clusters (σ_{rel} in 10^{-36} m^2 sr^{-1}), (d) IR prediction for mixed clusters (I_{rel} in km mol^{-1}), (e) IR prediction for pure clusters (I_{rel} in km mol^{-1}), (f) FTIR-jet ($A = \ln(\frac{I_0}{I})10^3$). For the scaling procedure, see Section 2.4. In the trimer case, the most stable MP2-M structure with two equal molecules pointing into the same direction is used for the stick spectra.

band is observed, whereas the predicted red shift of **wm** matches the new band emerging in the mixed system. The associated intensity transfer from the relaxation of **mw** into **wm** is indicated by dotted arrows and lines in Fig. 4c. This conformational preference is in agreement with most quantum

chemical calculations[18,21,40,47,54,55] (but not at the B3-S and MP2-S levels) as well as microwave spectroscopy investigations.[7] In cryogenic argon matrices, **wm** is also found to be the most stable dimer isomer,[8,54] whereas nitrogen matrices change this donor/acceptor preference.[8,56] Diffusion Monte Carlo simulations for **wm** and **mw** have shown that the stability of the mixed dimers also depends on the zero point energy for the hindered internal rotation of the monomers.[21] The methanol hydroxy group is engaged in the hydrogen bond in **mw**, thus its torsion mode is more restricted than in **wm** and blue-shifted. Its contribution to the zero point energy is thus strongly augmented, which contributes to the reduced stability of **mw** compared to **wm**.

In the central part of Fig. 2 the **wm** dimer region from a Raman measurement with relative concentration of **m** : **w** ≈ 1 : 3 (magnified by a factor of five) is also shown. The **wm** band persists, whereas the **mm** band decreases compared to the spectrum with a **m** : **w** ratio of 3 : 1. By taking a closer look at the **wm** band one notices a splitting of ~2.5 cm^{-1} between a more intense band at 3568.0 cm^{-1} and a less intense one at 3565.5 cm^{-1}. This splitting is not resolved in the corresponding IR spectrum due to more extensive rotational contours. Since the splitting cannot be traced back to conformational or donor–acceptor isomerism (*vide supra*), a tunneling process is the probable cause. To further investigate this hypothesis, measurements with O-deuterated methanol and deuterium oxide were carried out. Raman jet spectra of the OD stretching region are shown in Fig. 5. The theoretical prediction shown in Fig. 6 is again unambiguous in terms of the donor/acceptor preference. The corresponding **wm** band was observed at 2611 cm^{-1}. No splitting can be resolved in the OD stretching spectra. Therefore, a mass-independent cause for the splitting in the OH stretching region can be excluded. The most likely reason for the splitting seems to be an exchange of the water donor between the methanol acceptor lone pairs.

This exchange could proceed *via* intramolecular torsion of the methanol OH group, but a lower energy pathway involves more or less rigid rotation of the methanol unit with respect to the hydrogen bond from the water. This may be described by the departure of the methanol OH group from the plane of the heavy atoms, or else by the torsional angle Φ_{HCOO} between these four atoms, where the last O stands for the water oxygen.

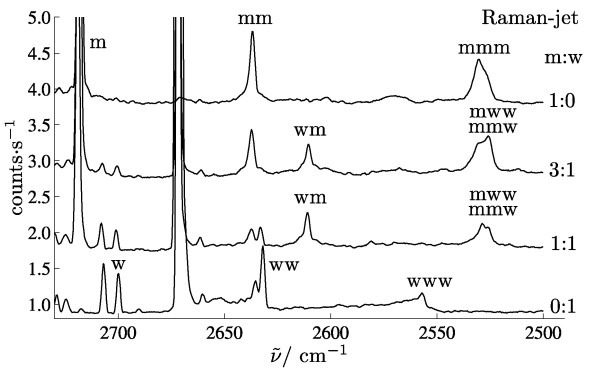

Fig. 5 Raman-jet spectra of the mixed deuterated methanol–deuterium oxide system in the OD stretching region.

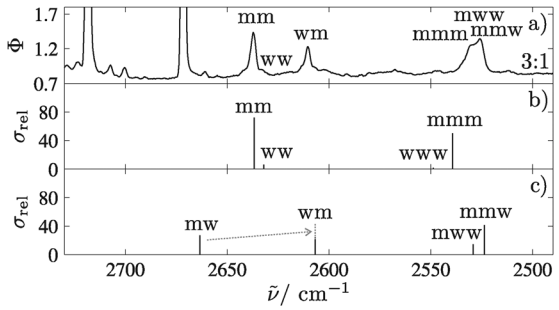

Fig. 6 Comparison of calculated (MP2-S/MP2-M average) and experimental Raman spectra of pure and mixed dimers and trimers of the deuterated methanol–deuterium oxide system: (a) Raman-jet (Φ in s^{-1}), (b) Raman prediction for pure clusters (σ_{rel} in 10^{-36} m^2 sr^{-1}), (c) Raman prediction for mixed clusters (σ_{rel} in 10^{-36} m^2 sr^{-1}). For the scaling procedure, see Section 2.4.

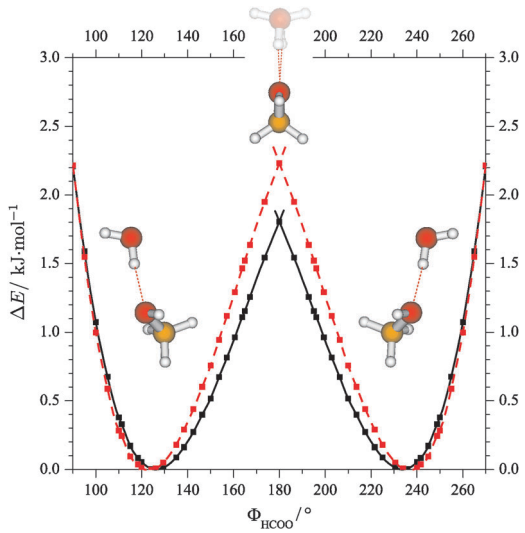

Fig. 7 Lone pair switching process between enantiomeric water–methanol dimer configurations with (dashed line, red) and without (full line, black) hydrogen-bonded OH stretching excitation, illustrating that OH stretching excitation will slow down the tunneling process. See text for details.

Explorative calculations have been carried out along this internal coordinate path at the B3-S level. The corresponding curves are shown in Fig. 7. The electronic energy (solid black line) and the energy including harmonic OH donor stretching vibration (red dashed line) of the hydrogen bonded water molecule are shown. Relative energies ΔE/kJ mol^{-1} with respect to the corresponding minimum of the given curve are illustrated (*i.e.* the red curve is shifted downwards by 43.3 kJ mol^{-1}).

At 180° there is a cusp in this particular internal coordinate mapping. This is due to the fact that this structure occurs in the form of two enantiomers, like the minima. They are connected by a swing of the dangling water OH from one side to the other. For the C_s-symmetric structure, where the dangling water OH points upwards, a second imaginary frequency is obtained. This means that the complex is unlikely to pass through an achiral structure when switching the hydrogen-bonded lone electron pairs.[57] A proper transition

state analysis would have to include at least two torsional angles and would lead over cusp-free, true transition states.

Upon water OH stretching excitation, the effective barrier to inversion is seen to increase from about 1.8 to 2.2 kJ mol^{-1} in this simplified model. At the same time, the barrier is broadened. Therefore, one qualitatively expects a lowering of the tunneling splitting upon OH stretching excitation. Assuming that only the $l \leftarrow l$ and $u \leftarrow u$ transitions are observed (where l refers to the lower and u to the upper state of the tunneling doublet in the ground and vibrationally excited states), the experimental data indicate that the tunneling splitting decreases by 2.5 cm^{-1} with respect to the vibrational ground state. Thus, the ground state splitting must be larger than 2.5 cm^{-1}. The relative weakness of the lower frequency transition together with an expected torsional temperature $T > 10$ K in the jet indicates a substantially larger value. In comparison, for the *tert*-butyl alcohol–water dimer a ground state splitting of 1.5 cm^{-1} with a barrier of 5.4 kJ mol^{-1} was found by Evangelisti and Caminati.[58] It is also evident that deuteration will slow down the process well below our spectral resolution, in agreement with the experimental finding and with an order of magnitude decrease in the case of *tert*-butyl alcohol and water.[58]

One should emphasize that our conclusion rests on two assumptions—the dominance of transitions which do not change the tunneling symmetry (plausible in a Franck–Condon like picture) and the near-proportionality of the intensity to the lower state population (plausible if the wavefunction amplitude is small at the transition state). For a more complete description of the process, multidimensional calculations will be needed.[59] However, the reduced dimensionality picture in Fig. 7 already provides qualitative support for the interpretation of the unexpected splitting of the mixed **wm** dimer peak in Fig. 2, which is largely quenched upon deuteration.

After having understood the mixed dimer region of methanol–water mixtures, we can switch to the more challenging trimer signatures which are shifted further to low frequency. Due to their cyclic, quasisymmetric nature[60–66], one expects largely different Raman and IR intensities for the individual OH stretching bands. Concerted stretching[34] leads to the lowest frequency band with a large change in polarizability. The IR intensity profits from out-of-phase vibration of the three coupled oscillators. There is no obvious localization of the vibrational amplitude on either water or methanol. To discriminate among trimers of different compositions, Raman-jet results for different ratios of water and methanol are shown in the box in the upper-right corner in Fig. 2. Adding small amounts of water to methanol leads to the appearance of a band at 3425 cm^{-1} (**mmw**). With more water, a mixed trimer band at 3440 cm^{-1} is observed (**mww**). This **mww** feature can also be found in the FTIR-jet spectra at 3439 cm^{-1}, together with at least two new trimer bands which require quantum chemical predictions for a tentative assignment.

There is considerable isomerism expected for mixed methanol–water trimers despite the complete absence of competitive non-cyclic structures, as inferred experimentally from the analogous methanol case[17] and theoretically in many studies.[18,22,23,25,42] This is somewhat different when a benzene chromophore is attached. In all cases, one unit points (arbitrarily) above the hydrogen bonded ring (u) and two below (d) in the most stable structure. At the B3LYP level, the two d units preferentially belong to different species, whereas MP2 calculations predict the two d units to be the same in the most stable variant (see Table 3). However, the differences are only on the order of 0.1 to 0.3 kJ mol^{-1} and we will concentrate on the MP2 preference in the following. The full set of trimer results is summarized in Tables S12 and S13 (ESI†) and extended to tetramers in Table S15 (ESI†). There is a systematic increase of the trimer dissociation energy with increasing methanol content, as expected based on dispersion energy contributions and also the trend in the dimers. We note that the B3-S approach almost fails in reproducing this trend (Table 3).

Table 3 Differences of zero point corrected dissociation energies of pure and mixed methanol–water trimers ΔD_0 in kJ mol^{-1}. Numbers in parentheses refer to the O-deuterated clusters

	$\mathbf{w}_d\mathbf{w}_d\mathbf{w}_u$	$\mathbf{m}_d\mathbf{w}_d\mathbf{w}_u$	$\mathbf{m}_u\mathbf{w}_d\mathbf{w}_d$	$\mathbf{m}_d\mathbf{m}_u\mathbf{w}_d$	$\mathbf{m}_d\mathbf{m}_d\mathbf{w}_u$	$\mathbf{m}_d\mathbf{m}_d\mathbf{m}_u$
B3-S	0.00	−1.03 (−0.29)	−0.88 (−0.50)	−1.48 (−1.18)	−1.30 (−1.25)	−1.82 (−2.08)
MP2-S	0.00	−2.27 (−1.26)	−2.59 (−1.48)	−4.83 (−2.48)	−4.92 (−2.69)	−7.26 (−3.72)
MP2-M	0.00	−4.16 (−3.06)	−4.39 (−3.20)	−8.41 (−6.09)	−8.58 (−6.31)	−12.85 (−9.44)
MP2-L	0.00	−5.24 (−4.26)	−5.48 (−4.30)	−10.68 (−8.54)	−10.81 (−8.73)	−16.21 (−13.09)

The quality of the harmonic wavenumber predictions can be tested for the Raman active bands, which are straightforward to assign based on the experimental data. There, one finds a large wavenumber shift from **www** to **mww** followed by smaller shifts in the same direction for **mmw** and **mmm**. This is not fully reflected in the MP2 prediction shown in Fig. 4, where **mmw** even overshoots **mmm** slightly. However, the predicted shifts are within 20–30 cm^{-1} of experiment, which is reasonable at this elementary level of treatment.

As shown in traces (d) and (e) of Fig. 4, the IR situation is considerably more congested, with up to 8 new trimer transitions expected due to the lifting of the C_3 symmetry degeneracy. Trace (e) shows that the calculations overestimate this degeneracy lifting. For **mmm**, the predicted splitting of 21 cm^{-1} is to be compared to the experimental one of 5 cm^{-1}.[17] With this and the general error bar of ~20–30 cm^{-1} in mind, we propose some mixed assignments of the three trimer bands which fall in the region between the dimer absorption and the Raman active trimer bands (see Table 1). The band at 3533 cm^{-1} is expected to have **www** contributions,[67] but may derive most of its intensity from **mmw**. The band at 3514 cm^{-1} is likely to have contributions from both mixed trimers. However, one can clearly see that the Raman active bands are less ambiguous.

In the case of O-deuterated methanol co-expanded with deuterium oxide only one new band is present in the trimer region of the Raman-jet measurements (see Fig. 5). No other band appears when changing the ratio of deuterated methanol and deuterium oxide. A comparison of experimental and calculated spectra is shown in Fig. 6. One can notice that the mixed trimers (**mww** and **mmw**) are predicted near the turning point of the **www** → **mmm** sequence, lower in wavenumber

than **mmm** and closely neighboured. Therefore, the mixed band at 2536 cm^{-1} can tentatively be assigned to overlapping mixed trimers. One can see that the overshooting red shift of mixed clusters, which was already predicted at some levels for non-deuterated mixtures (see Table S13, ESI†) but not observed in the experiment, is fully developed after deuteration in both experiment and theory. It points at substantial excess effects in the mixtures, which will be discussed in Section 3.4.

3.2 Ethanol–water

Fig. 8 displays a survey of the Raman- as well as the FTIR-jet spectrum of the mixed ethanol–water system. The Raman-jet spectrum was recorded at an estimated ethanol : water concentration ratio of 1 : 1, whereas the ethanol : water ratio in the FTIR-jet spectrum is approximately 2 : 1. Assignments of the observed bands are summarized in Table 2. In analogy to the methanol–water system, mixed dimer bands are present in the Raman and FTIR-jet spectra. However, while the Raman spectrum shows two peaks at 3551 and 3548 cm^{-1}, the former is only a weak shoulder in the FTIR spectrum. It is caused by a metastable conformation, which is relaxed into the more stable conformation due to the larger average nozzle distance and therefore colder expansion in the FTIR experiment. The mixed dimer band at a lower wavenumber is due to a *gauche* ethanol acceptor subunit, whereas the band at higher wavenumbers is assigned to a *trans* acceptor (see ref. 9). In the left inset in Fig. 8 the acceptor region of *trans* ethanol is shown for Raman measurements without (top) and with (bottom) 5% argon. In the lower central inset of Fig. 8 the hydrogen-bonded OH stretching bands are shown. The intensity of the $\mathbf{we}_t$ band at 3551 cm^{-1} decreases along with the acceptor band of *trans* ethanol when the heavier collider argon is added, showing that $\mathbf{we}_{g+}$ is more stable. Assuming a conservative lower limit of the effective conformational temperature in the argon expansion of 10 K and at most 10% remaining $\mathbf{we}_t$ fraction, one can derive a lower limit for the energy difference between $\mathbf{we}_t$ and $\mathbf{we}_{g+}$ of 0.2 kJ mol^{-1} from the Boltzmann population. These assignments are also supported by quantum chemical calculations (see Fig. 9 and Table S18, ESI†). At all levels of calculation five mixed ethanol–water dimer configurations can be optimized. Relative stabilities as well as local minimum structures are illustrated in Fig. 10. In the three most

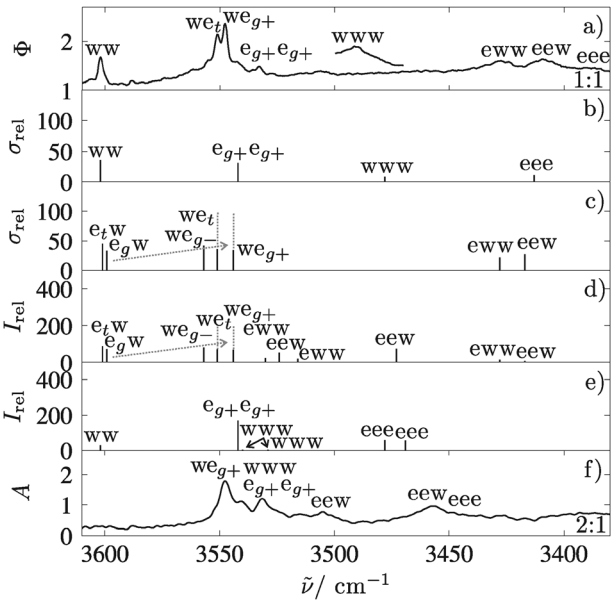

Fig. 9 Comparison of calculated (MP2-S/MP2-M average) and experimental Raman and FTIR spectra of pure and mixed dimers and trimers of the ethanol–water system: (a) Raman-jet (Φ in s^{-1}), (b) Raman prediction for pure clusters (σ_{rel} in 10^{-36} m^2 sr^{-1}), (c) Raman prediction for mixed clusters (σ_{rel} in 10^{-36} m^2 sr^{-1}), (d) IR prediction for mixed clusters (I_{rel} in km mol^{-1}), (e) IR prediction for pure clusters (I_{rel} in km mol^{-1}), (f) FTIR-jet ($A = \ln(\frac{I_0}{I})10^3$). For the scaling procedure, see Section 2.4.

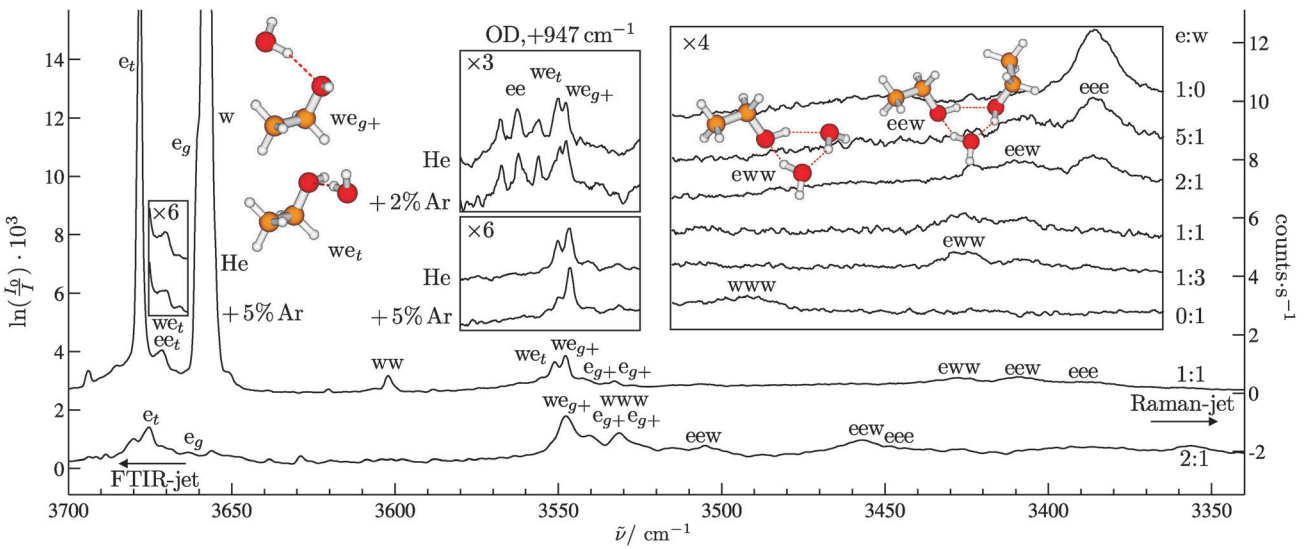

Fig. 8 Raman- and FTIR-jet spectra of the mixed ethanol–water system in the OH (and OD) stretching region. Absorbance magnification factors are shown in the insets, which share the wavenumber scale of the main spectra. The bottom left inset shows relaxation of $\mathbf{we}_t$ to $\mathbf{we}_{g+}$ by adding Ar. The top left inset shows the same in the OD region (shifted in wavenumber to match the $\mathbf{we}_{g+}$OH spectrum). The right inset shows the evolution of mixed trimers with increasing ethanol-to-water ratio.

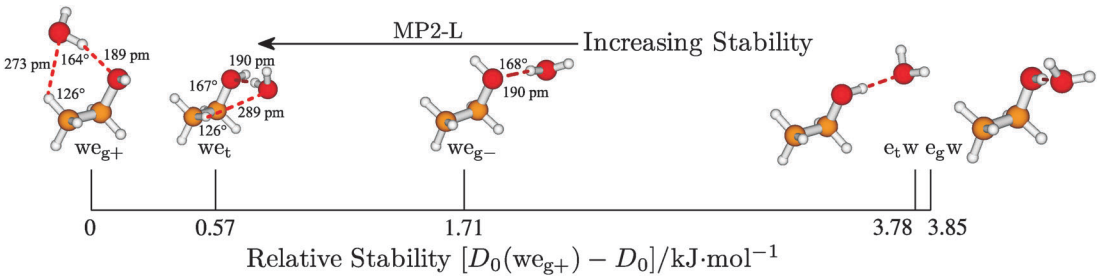

Fig. 10 Structures and relative stabilities of **we**/**ew** dimer isomers at the MP2-L level. Secondary hydrogen bond-like CH···O contacts and hydrogen bond lengths, as well as the O–H···O angles are indicated.

stable structures, water acts as the hydrogen bond donor. In these cases, not only the conformation of ethanol (*trans* or *gauche*) is relevant, but also the choice of the acceptor lone pair (see Section 2.3). As illustrated in Fig. 10, **we**$_{g+}$ (with a hydrogen bond to the right lone pair of ethanol) is calculated to be the most stable and most compact mixed dimer at the MP2-L level. In contrast to **we**$_{g-}$ it is stabilized by a secondary hydrogen bond-like interaction between a C–H group and the water oxygen. It bends the primary hydrogen bond slightly further away from the linear arrangement. The enhanced stability of **e**$_g$ in this complex parallels the one observed for ethanol dimers,[34,37,39] as does the enhanced red shift. The donor–acceptor roles of ethanol and water in a matrix are analogous to those of methanol and water, with **we** being the more stable one in argon and **ew** in nitrogen.[8] In the jet, **ew** dimers are expected to relax into the more stable structures, as implied by the intensity shifts postulated in Fig. 9 by the dotted lines. The **we**-splitting shrinks by a factor less than 2 upon OD deuteration of both ethanol and water (see Fig. 8). Theory predicts this factor to be 1.3 (MP2-L). Furthermore, the relaxation behavior is analogous to that of the non-deuterated dimer, although less pronounced because a smaller amount of argon is added. Therefore, it is clear that the **we**-splitting is not due to tunneling—as in **wm**—but rather due to conformational isomerism.

To assign the trimer bands in the Raman-jet spectra, concentration variation was applied (see ref. 9 and the rightmost box in Fig. 8 with improved relative concentration estimates). In analogy to the mixed methanol–water trimer bands, the intensity of the band at a higher wavenumber increases with an increasing content of water while the more red-shifted band increases with the relative ethanol content. As supported by the calculations in Fig. 9 (and Table S16, ESI†), the band at 3427 cm^{-1} can be assigned to **eww** while the band at 3409 cm^{-1} corresponds to **eew**. Isomerism does not scramble the coarse-grained sequence from **www** over **eww** and **eew** to **eee** in the spectrum. The stability of the trimers (Table 4) increases with an increasing alcohol content (except for the B3-S level), see also ref. 25. Again, the most stable configurations appear to be those with equivalent molecules pointing in the same direction relative to the ring plane, but the preference is weak. Trimers containing *trans* ethanol tend to be more stable than those containing the *gauche* conformation, but no systematic exploration was attempted. At the MP2-M and MP2-L levels only trimers containing *trans* ethanol with two equal molecules pointing into the same direction were calculated and plotted (Fig. 9). Unlike in the methanol–water case, the prediction of the trimer sequence matches the experimental one in its qualitative behavior. There is no overshooting of the red shift as a function of the alcohol content, before the pure alcohol value is reached. However, the size of the shifts is underestimated towards high ethanol content.

Table 4 Differences of zero point corrected dissociation energies of pure and mixed ethanol–water trimers ΔD_0 in kJ mol^{-1}

	$\mathbf{w}_d\mathbf{w}_d\mathbf{w}_u$	$\mathbf{e}_{g,d}\mathbf{w}_d\mathbf{w}_u$	$\mathbf{e}_{t,d}\mathbf{w}_u\mathbf{w}_d$	$\mathbf{e}_{g,u}\mathbf{w}_d\mathbf{w}_d$	$\mathbf{e}_{t,u}\mathbf{w}_d\mathbf{w}_d$
B3-S	0.00	+0.75	+0.29	+0.60	−0.42
MP2-S	0.00	−1.65	−1.69	−2.41	−2.79
MP2-M	0.00				−5.32
MP2-L	0.00				−6.65

	$\mathbf{e}_{g,u}\mathbf{e}_{g,d}\mathbf{w}_d$	$\mathbf{e}_{g,d}\mathbf{e}_{g,u}\mathbf{w}_d$	$\mathbf{e}_{g,d}\mathbf{e}_{t,u}\mathbf{w}_d$	$\mathbf{e}_{t,d}\mathbf{e}_{t,u}\mathbf{w}_d$	$\mathbf{e}_{t,d}\mathbf{e}_{t,d}\mathbf{w}_u$	$\mathbf{e}_{t,d}\mathbf{e}_{t,d}\mathbf{e}_{t,u}$
B3-S	+0.96	+0.87	−0.15	−0.06	+0.08	+0.30
MP2-S	−4.83	−4.85	−5.20	−5.30	−5.60	−8.09
MP2-M					−11.02	−16.91
MP2-L					−13.59	

As Fig. 9 illustrates, the IR absorption cross section of the Raman active trimer bands involving synchronous OH stretching motion is too low to make them detectable. Instead, there are a few stronger bands predicted at higher wavenumbers. For example, the band at 3457 cm^{-1} may correspond to **eew**, as may the band at 3505 cm^{-1}. Overall, the IR spectra are more ambiguous to assign due to the higher congestion. More reliable quantum chemical predictions would be helpful.

3.3 Donor/acceptor quality analysis

Experimental spectra as well as sufficiently high level theoretical calculations show that **wa** is more stable than **aw** for **a** = **m** and for **a** = **e**$_{g+}$, **e**$_{g-}$, **e**$_t$. This can further be analyzed by donor and acceptor strengths according to eqn (6) and (7). Calculated dimer values on different levels are summarized in Table 5. ΔE_D turns positive at the higher levels of calculation. Water is a weak donor compared to methanol and ethanol but it also is a much weaker acceptor and the latter effect clearly dominates. Thus, both alcohols can be considered as relatively good donors in mixed aggregates with water, but their acceptor strength exceeds their donor strength. Therefore, mixed complexes with water acting as the donor and the alcohol as an acceptor are found to be more stable, consistent with the spectroscopic findings.

Table 5 Relative donor ($D_{\mathbf{wa}}$) and acceptor strengths ($A_{\mathbf{wa}}$) of water in mixed alcohol–water dimers in kJ mol^{-1}, isomer differences (ΔE_D) in kJ mol^{-1} (all including harmonic zero point energy correction) and relative acceptor strengths of water based on calculated wavenumbers ($A_{\mathbf{wa}}^{\mathrm{spec}}$) in cm^{-1}. Zero point corrected dissociation energies with respect to the monomer conformation realized in the given cluster were used for calculations

	$D_{\mathbf{wa}}$	$A_{\mathbf{wa}}$	ΔE_D	$A_{\mathbf{wa}}^{\mathrm{spec}}$
B3-S				
wm	−1.4	−0.4	−1.0	−26
we$_t$	−0.8	−0.3	−0.5	−32
we$_{g+}$	−0.3	−1.1	+0.8	−39
we$_{g-}$	−0.5	−1.0	+0.5	−34
MP2-S				
wm	−2.8	−1.8	−1.0	−33
we$_t$	−3.1	−2.9	−0.3	−44
we$_{g+}$	−3.8	−4.3	+0.5	−54
we$_{g-}$	−4.6	−3.5	−1.1	−46
MP2-M				
wm	−2.7	−3.5	+0.8	−44
we$_t$	−3.2	−5.4	+2.2	−58
we$_{g+}$	−3.8	−6.8	+3.0	−61
we$_{g-}$	−4.7	−5.9	+1.2	−57
MP2-L				
wm	−2.8	−4.5	+1.7	−42
we$_t$	−3.5	−6.7	+3.2	−54
we$_{g+}$	−4.1	−7.9	+3.8	−58
we$_{g-}$	−4.9	−7.1	+2.1	−54

Table 5 also shows that the acceptor strength of ethanol is consistently higher than that of methanol in mixed aggregates with water. This can be explained by the higher electron density at the ethanol oxygen, which is caused by the stronger inductive effect (+I-effect) from its ethyl group compared to the methyl group in methanol. The donor strength also increases with the size of the alkyl group, but not as much. The acceptor strength varies with the ethanol conformation, with **g+** being the strongest acceptor, **t** having medium, and **g−** having the lowest acceptor strength. This is most likely a consequence of the weak C–H···O interaction, which cooperatively strengthens the water-to-ethanol hydrogen bond in **we**$_{g+}$ and **we**$_t$.

One can see from Table 5 that low level calculations underestimate the energetic donor strength and even more the acceptor strength of alcohols relative to water. This can lead to a wrong prediction of the energy sequence. The spectroscopic acceptor strengths are found to be more robust with respect to the computational level. They also correlate rather nicely with the experimental **ww**–**wa** shifts (−35 cm^{-1} for **wm**, −51 cm^{-1} for **we**$_t$, and −54 cm^{-1} for **we**$_{g+}$). Furthermore, the $A_{\mathbf{wa}}^{\mathrm{spec}}$ sequence **we**$_{g+}$ > **we**$_t$ > **we**$_{g-}$ > **wm** corresponds to the energy scale (see Fig. 10), whereas the energy quantity $A_{\mathbf{wa}}$ predicts **e**$_{g-}$ to be the better acceptor than **e**$_t$. This may be related to the global property of $A_{\mathbf{wa}}$, which involves OH/CH competition for the electron density at the water molecule in **e**$_g$**w**, among other things.

3.4 Excess enthalpies

Under ideal conditions one would expect a linear dependence of the OH stretching red shift on the alcohol content $x_{\mathbf{a}}$ for the mixed clusters. The ideal donor wavenumber of the mixed dimers would be midway between the positions of the pure dimers. The mixed trimers would be shifted from **www** by 1/3 for **aww** and 2/3 for **aaw** trimers in the direction of **aaa**. However, the experimental red shift is found to be nonlinear, which is most apparent in the case of the Raman active trimer bands in the sequence from pure water to pure alcohol trimers (see Fig. 2, 5, and 8). It is also seen in the methanol–water dimer case, where the mixed dimer absorbs at a lower wavenumber compared to the methanol and ethanol dimers, instead of absorbing between the two. For ethanol, this overshooting is not achieved, because the **ww** and **ee** wavenumbers are further apart. Still, the mixed dimers do not appear midway between **ww** and **ee**. This non-linearity can be described by an excess wavenumber shift $\Delta_E\tilde{\nu}$

$$\Delta_E\tilde{\nu}(x_{\mathbf{a}}) = \tilde{\nu}(x_{\mathbf{a}}) - [\tilde{\nu}(x_{\mathbf{a}} = 0) + (\tilde{\nu}(x_{\mathbf{a}} = 1) - \tilde{\nu}(x_{\mathbf{a}} = 0))x_{\mathbf{a}}] \quad (10)$$

which is negative if the mixed cluster shift exceeds the interpolated one. The excess wavenumbers of both systems are

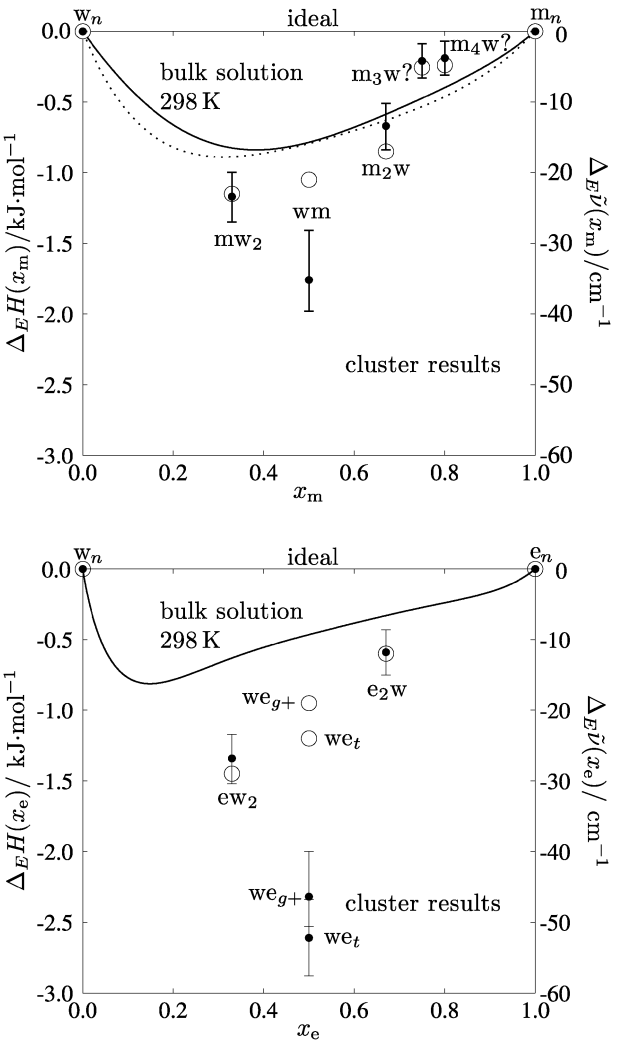

Fig. 11 Excess enthalpies (left scale, black dots with error bars) and excess wavenumbers (right scale, open circles, similar error bars omitted) of the mixed methanol–water system (top) and mixed ethanol–water system (bottom) in comparison to experimental excess enthalpies of bulk solutions at room temperature (full and dashed lines[3,45,69] interpolated). Error bars derive from estimated wavenumber uncertainties.

illustrated as open circles in Fig. 11. The more negative the value of the excess wavenumber for a given cluster, the more favorable the corresponding **a**/**w** combination.

Hydrogen bond enthalpies have been correlated with the hydrogen bond induced red shifts $\Delta\tilde{\nu}$ of the observed cluster band positions relative to the monomers.[29] These hydrogen bond-induced red shifts are straightforward to determine in the isolated OH chromophore of alcohols. In the case of water a coupling between the symmetric (3657 cm^{-1}) and antisymmetric vibrations (3756 cm^{-1}) exists in the monomer[16] and is progressively detuned by hydrogen bonding in the clusters. To account for this coupling, two modifications regarding the red shift were applied. First of all, the average of the symmetric and antisymmetric band positions of the water monomer was used as a reference point for the localized OH stretching mode. Relative to this reference, initial red shifts $\Delta\tilde{\nu}$ of the observed cluster positions were calculated. To account for residual coupling in the cluster vibrations, a simple decoupling approach[68] was used to determine a deperturbed red shift $\delta\tilde{\nu}$:

$$2\Delta\tilde{\nu} = \delta\tilde{\nu} + \sqrt{4W^2 + (\delta\tilde{\nu})^2} \qquad (11)$$

Here, $W = 49.5\ cm^{-1}$ is one half of the difference between the symmetric and antisymmetric monomer positions. In mixed trimers and higher clusters both alcohol and water act as donors. Therefore, a weighted red shift reference according to the number of alcohol and water units was used. For mixed ethanol–water trimers a *trans* ethanol conformation was assumed.

According to Iogansen,[29] the hydrogen bond enthalpy ΔH can be estimated from the red shift $\delta\tilde{\nu}$ relative to the free monomer as:

$$\Delta H_{\log}/(kJ\,mol^{-1}) \approx -1.3\sqrt{(\delta\tilde{\nu}/cm^{-1})} \qquad (12)$$

In analogy to the excess wavenumbers, excess enthalpies can be calculated from these estimated enthalpies:

$$\Delta_E H(x_{\mathbf{a}}) = \Delta H(x_{\mathbf{a}}) - [\Delta H(x_{\mathbf{a}} = 0) + (\Delta H(x_{\mathbf{a}} = 1) - \Delta H(x_{\mathbf{a}} = 0))x_{\mathbf{a}}] \qquad (13)$$

The results are listed in Tables 1 and 2 (for more details, see Tables S17 and S18, ESI†). Due to approximations involved, only qualitative conclusions should be drawn. The curves in Fig. 11 confirm that water rich mixtures are energetically favored over alcohol rich mixtures. For both systems, the trend of excess wavenumbers (open circles) and enthalpies (black dots) matches the shape of the bulk solution excess enthalpy at room temperature.[3,45,69] The cluster excess quantities are asymmetric, like their bulk counterparts. In the case of mixed dimers, the Iogansen analysis overshoots systematically. This indicates that the relationship between enthalpy and wavenumber shift does not span non-cooperative and cooperative hydrogen bonds in the same way. Otherwise, an excess enthalpy of $\sim$1 kJ mol^{-1} appears to correspond to an excess wavenumber shift of 20 cm^{-1}. Not surprisingly, the absolute values of the cluster excess quantities are larger than those measured at room temperature, because thermal weakening effects are absent. However, it is rewarding to see that there is a qualitative correspondence.

Table 6 Trends in several properties of ethanol–water dimers as a function of decreasing C–H···O distance d(C–H···O). $\Delta\tilde{\nu}_{\mathbf{w}}$ is the hydrogen-bonded OH stretching red shift relative to the water dimer and ΔE_0 is the ground state energy difference relative to $\mathbf{we}_{g+}$

Property	$\mathbf{we}_{g-}$	$\mathbf{we}_{t}$	$\mathbf{we}_{g+}$	Method
d(C–H···O)/pm	529	289	273	MP2-L
$\Delta\tilde{\nu}_{\mathbf{w}}/cm^{-1}$		−51	−54	exp.
$\Delta\tilde{\nu}_{\mathbf{w}}/cm^{-1}$	−49	−56	−58	MP2-L
ΔE_0/kJ mol^{-1}	$\gg$0.2	>0.2	0	exp.
ΔE_0/kJ mol^{-1}	1.71	0.14	0	MP2-L

Note that the methanol diagrams also contain tentative results for $\mathbf{m}_3\mathbf{w}$ and $\mathbf{m}_4\mathbf{w}$. These have been obtained from spectra recorded for the methanol tetramer (3212 cm^{-1}) and pentamer (3167 cm^{-1}), when small amounts of water are added (see Table 1). They confirm the low exothermicity observed when adding small amounts of water to liquid methanol. Water-rich tetramers and pentamers are below the detection limit of our current setup due to the poor scattering power of water and the competition from the pure water cluster. It will be interesting to correlate the cluster-resolved findings in this work to bulk IR and Raman spectra as a function of the alcohol content.[70]

3.5 Quantifying the effect of a weak C–H···O hydrogen bond

The series $\mathbf{we}_{g-}$–$\mathbf{we}_{t}$–$\mathbf{we}_{g+}$, of which the last two members have been characterized experimentally in the present work, allows for a quantification of the effect which the weak interaction between a terminal C–H and the lone pair of the water molecule (see Fig. 10) has on the properties of the water–ethanol complex. Table 6 summarizes some of these effects, both experimentally and also based on MP2-L calculations, in particular where experimental data are not available.

Structurally, $\mathbf{we}_{g-}$ has no C–H···O contact (d > 0.5 nm), whereas $\mathbf{we}_{t}$ has a long one (0.29 nm) and $\mathbf{we}_{g+}$ a shorter one (0.27 nm), according to the calculations. This is reflected by the experimental and calculated red shift of the donor OH relative to the water dimer $\Delta\tilde{\nu}_{\mathbf{w}}$, which increases significantly from $\mathbf{we}_{g-}$ (only calculation) to $\mathbf{we}_{t}$ and slightly further for $\mathbf{we}_{g+}$. Furthermore, the experimental data suggest that $\mathbf{we}_{t}$ is at least 0.2 kJ mol^{-1} higher in energy than $\mathbf{we}_{g+}$ (based on the successful depletion with argon) whereas $\mathbf{we}_{g-}$ is much higher, based on its absence in the jet.

As one can see, the effects induced by the weak hydrogen bond between the C–H group and the oxygen lone electron pair are clearly detectable, but still fairly subtle. They may become stronger in longer chain alcohols with limited water miscibility,[71] and certainly in larger, more water-rich clusters. Whether they should be classified as hydrogen bonds or subtle electrostatic and dispersion interactions remains a matter of definition.

4. Conclusions and outlook

Dimers and trimers composed of water and either methanol or ethanol were studied by Raman and FTIR spectroscopy in supersonic jets, complemented by simple harmonic quantum

chemical calculations to explore their limitations in reproducing the OH (OD) stretching manifold.

Among the most important conclusions are:

(i) In mixed dimers, water assumes the role of the hydrogen bond donor, not because it is the better donor than methanol or ethanol, but because it is a much inferior acceptor.

(ii) There is multiple evidence for a rapid lone-pair switching process in water–methanol dimer which is slowed down substantially by exciting the hydrogen-bonded OH stretching fundamental or by deuteration.

(iii) Water forces ethanol into its less stable *gauche* conformation upon dimerization and it does so in such a way that it can profit from interaction with a C–H bond of the methyl group. This interaction was quantified from the experimental and some theoretical data.

(iv) When mixing water and alcohol in a cluster, the hydrogen-bonded OH vibration absorbs to the red of the position interpolated between the pure water cluster and the pure alcohol cluster. The resulting excess wavenumbers correlate qualitatively with excess enthalpies of bulk mixtures, consistent with a significant portion of the thermodynamic excess being rooted in small cluster hydrogen bonding.

(v) Where the pure water and alcohol clusters absorb in close vicinity to each other (water–methanol dimer, deuterium oxide–deuterated methanol dimers and trimers), the mixed clusters even absorb at a lower wavenumber than either of them, due to the large size of the excess wavenumber shift.

(vi) Medium-sized harmonic MP2 calculations are able to predict some coarse trends, but a high level anharmonic treatment and a proper treatment of basis set incompleteness effects would be needed to reproduce the spectra faithfully, in particular the congested FTIR spectra. The B3LYP/6-311+G(d) approach fails even qualitatively in most energetic and spectroscopic sequences when replacing water by alcohol.

In the future, it will be interesting to see how to see how an increase in the aliphatic chain length[31] affects the hydrogen bonds by introducing competing dispersion interactions. Also, it will be of interest to study highly polar fluorinated alcohols[72] in combination with water.[73]

Most importantly, the present work should pave the way for a rigorous theoretical treatment of ethanol/water, arguably the most popular liquid mixture. Beyond the pair potential and rigid monomer approximations customary in this field, it provides experimental benchmarks for a many-body expansion approach. A quantum chemical and dynamical treatment which is able to reproduce the conformational preferences and vibrational dynamics of mixed dimers and trimers has good prospects in a reliable and consistent description of the bulk solution of ethanol in water or of mesoscopic phenomena like ethanol/water nucleation.[74]

Acknowledgements

We thank Z. Xue and P. Zielke for experimental support in the early phase of this study. This work was supported by the DFG (grant Su121/2 and research training group GRK 782 (www.pcgg.de)) and by the FCI. R. Wugt Larsen acknowledges a fellowship grant from the Danish Research Council.

References

1 F. Franks and D. J. G. Ives, The structural properties of alcohol–water mixtures, *Q. Rev. Chem. Soc.*, 1966, **20**, 1–44.
2 G. L. Bertrand, F. J. Millero, C.-H. Wu and L. G. Hepler, Thermochemical Investigations of the Water–Ethanol and Water–Methanol Solvent Systems. I. Heats of Mixing, Heats of Solution, and Heats of Ionization of Water, *J. Phys. Chem.*, 1966, **70**, 699–705.
3 J. A. Larkin, Thermodynamic properties of aqueous non-electrolyte mixtures I. Excess enthalpy for water + ethanol at 298.15 to 383.15 K, *J. Chem. Thermodyn.*, 1975, **7**, 137–148.
4 J.-P. E. Grolier, Excess Volumes and Excess Heat Capacities of Water + Ethanol at 298.15 K, *Fluid Phase Equilib.*, 1981, **6**, 283–287.
5 G. C. Benson and O. Kiyohara, Thermodynamics of Aqueous Mixtures of Nonelectrolytes. I. Excess Volumes of Water-*n*-Alcohol Mixtures at Several Temperatures, *J. Solution Chem.*, 1980, **9**, 791–804.
6 M. A. Suhm, Hydrogen bond dynamics in alcohol clusters, *Adv. Chem. Phys.*, 2009, **142**, 1–57.
7 P. A. Stockmann, G. A. Blake, F. J. Lovas and R. D. Suenram, Microwave rotation-tunneling spectroscopy of the water–methanol dimer: Direct structural proof for the strongest bound conformation, *J. Chem. Phys.*, 1997, **107**, 3782–3790.
8 S. Coussan, P. Roubin and J. P. Perchard, Hydrogen bonding in ROH : R′OH (R, R′ = H, CH_3, C_2H_5) heterodimers: Matrix-dependent structure and infrared-induced isomerization, *J. Phys. Chem. A*, 2004, **108**, 7331–7338.
9 M. Nedić, T. N. Wassermann, Z. Xue, P. Zielke and M. A. Suhm, Raman spectroscopic evidence for the most stable water/ethanol dimer and for the negative mixing energy in cold water/ethanol trimers, *Phys. Chem. Chem. Phys.*, 2008, **10**, 5953–5956.
10 C. J. Gruenloh, F. C. Hagemeister, J. R. Carney and T. S. Zwier, Resonant Ion–Dip Infrared Spectroscopy of Ternary Benzene–$(Water)_n(Methanol)_m$ Hydrogen-Bonded Clusters, *J. Phys. Chem. A*, 1999, **103**, 503–513.
11 Y. Matsuda, A. Yamada, K. Hanaue, N. Mikami and A. Fujii, Catalytic Action of a Single Water Molecule in a Proton-Migration Reaction, *Angew. Chem., Int. Ed.*, 2010, **49**, 4898–4901.
12 Y. J. Hu, H. B. Fu and E. R. Bernstein, Infrared plus vacuum ultraviolet spectroscopy of neutral and ionic ethanol monomers and clusters, *J. Chem. Phys.*, 2006, **125**, 154305.
13 A. Amrein, M. Quack and U. Schmitt, High resolution interferometric Fourier transform infrared absorption spectroscopy in supersonic free jet expansions. A new technique for ultracold gaseous samples, *Z. Phys. Chem.*, 1987, **154**, 59–72.
14 D. Luckhaus, M. Quack, U. Schmitt and M. A. Suhm, On FTIR spectroscopy in asynchronously pulsed supersonic jet expansions and on the interpretation of stretching spectra of HF clusters, *Ber. Bunsen-Ges. Phys. Chem.*, 1995, **99**, 457–468.
15 T. Häber, U. Schmitt and M. A. Suhm, FTIR-spectroscopy of molecular clusters in pulsed supersonic slit-jet expansions, *Phys. Chem. Chem. Phys.*, 1999, **1**, 5573–5582.
16 G. Avila, J. M. Fernández, G. Tejeda and S. Montero, The Raman spectra and cross-sections of H_2O, D_2O, and HDO in the OH/OD stretching regions, *J. Mol. Spectrosc.*, 2004, **228**, 38–65.
17 R. Wugt Larsen, P. Zielke and M. A. Suhm, Hydrogen-bonded OH stretching modes of methanol clusters: A combined IR and Raman isotopomer study, *J. Chem. Phys.*, 2007, **126**, 194307.
18 M. Masella and J. P. Flament, Relation between cooperative effects in cyclic water, methanol/water, and methanol trimers and hydrogen bonds in methanol/water, ethanol/water, and dimethylether/water, *J. Chem. Phys.*, 1998, **109**, 7141–7151.
19 E. E. Fileti, P. Chaudhuri and S. Canuto, Relative strength of hydrogen bond interaction in alcohol-water complexes, *Chem. Phys. Lett.*, 2004, **400**, 494–499.
20 M. Ferrario, M. Haughney, I. R. McDonald and M. L. Klein, Molecular-dynamics simulation of aqueous mixtures: Methanol,acetone, and ammonia, *J. Chem. Phys.*, 1990, **93**, 5156–5166.
21 J. W. Moskowitz, Z. Bačić, A. Sarsa and K. E. Schmidt, Relative stabilities of the two isomers of the methanol-water dimer: The effects of the internal rotations of the hydroxyl and methyl groups of methanol, *J. Chem. Phys.*, 2001, **114**, 10294–10299.

22 S. M. Mejía, J. F. Espinal, A. Restrepo and F. Mondragón, Molecular Interaction of $(Ethanol)_2$–Water Heterotrimers, *J. Phys. Chem. A*, 2007, **111**, 8250–8256.
23 L. González, O. Mó and M. Yáñez, High level *ab initio* and density functional theory studies on methanol–water dimers and cyclic methanol$(water)_2$ trimer, *J. Chem. Phys.*, 1998, **109**, 139–150.
24 S. M. Mejía, J. F. Espinal and F. Mondragón, Cooperative effects on the structure and stability of $(ethanol)_3$–water, $(methanol)_3$–water heterotetramers and $(ethanol)_4$, $(methanol)_4$ tetramers, *THEOCHEM*, 2009, **901**, 186–193.
25 A. Mandal, M. Prakash, R. M. Kumar, R. Parthasarathi and V. Subramanian, *Ab initio* and DFT Studies on Methanol–Water Clusters, *J. Phys. Chem. A*, 2010, **114**, 2250–2258.
26 R. S. Ruoff, T. D. Klots, T. Emilsson and H. S. Gutowsky, Relaxation of conformers and isomers in seeded supersonic jets of inert gases, *J. Chem. Phys.*, 1990, **93**, 3142–3150.
27 T. Emilsson, T. C. Germann and H. S. Gutowsky, Kinetics of molecular association and relaxation in a pulsed supersonic expansion, *J. Chem. Phys.*, 1992, **96**, 8830–8839.
28 C. Emmeluth, V. Dyczmons and M. A. Suhm, Tuning the hydrogen bond donor/acceptor isomerism in jet-cooled mixed dimers of aliphatic alcohols, *J. Phys. Chem. A*, 2006, **110**, 2906–2915.
29 A. V. Iogansen, Direct proportionality of the hydrogen bonding energy and the intensification of the stretching ν(XH) vibration in infrared spectra, *Spectrochim. Acta, Part A*, 1999, **55**, 1585–1612.
30 O. Takahashi, Y. Kohno and M. Nishio, Relevance of Weak Hydrogen Bonds in the Conformation of Organic Compounds and Bioconjugates from Recent Experimental Data and High-Level *ab initio* MO Calculations, *Chem. Rev.*, 2010, **110**, 6049–6076.
31 T. N. Wassermann, P. Zielke, J. J. Lee, C. Cézard and M. A. Suhm, Structural Preferences, Argon Nanocoating, and Dimerization of *n*-Alkanols As Revealed by OH Stretching Spectroscopy in Supersonic Jets, *J. Phys. Chem. A*, 2007, **111**, 7437–7448.
32 C. A. Rice, N. Borho and M. A. Suhm, Dimerization of Pyrazole in Slit Jet Expansions, *Z. Phys. Chem.*, 2005, **219**, 379–388.
33 N. Borho, M. A. Suhm, K. Le Barbu-Debus and A. Zehnacker, Intra- *vs.* intermolecular hydrogen bonding: dimers of alpha-hydroxyesters with methanol, *Phys. Chem. Chem. Phys.*, 2006, **8**, 4449–4460.
34 P. Zielke and M. A. Suhm, Concerted proton motion in hydrogen-bonded trimers: A spontaneous Raman scattering perspective, *Phys. Chem. Chem. Phys.*, 2006, **8**, 2826–2830.
35 Z. Xue and M. A. Suhm, Probing the stiffness of the simplest double hydrogen bond: The symmetric hydrogen bond modes of jet-cooled formic acid dimer, *J. Chem. Phys.*, 2009, **131**, 054301.
36 Z. Xue, *Raman spectroscopy of carboxylic acid and water aggregates, PhD thesis*, Universität Göttingen, 2010.
37 T. N. Wassermann and M. A. Suhm, Ethanol Monomers and Dimers Revisited: A Raman Study of Conformational Preferences and Argon Nanocoating Effects, *J. Phys. Chem. A*, 2010, **114**, 8223–8233.
38 R. K. Kakar and C. R. Quade, Microwave rotational spectrum and internal rotation in *gauche* ethyl alcohol, *J. Chem. Phys.*, 1980, **72**, 4300–4307.
39 C. Emmeluth, V. Dyczmons, T. Kinzel, P. Botschwina, M. A. Suhm and M. Yáñez, Combined jet relaxation and quantum chemical study of the pairing preferences of ethanol, *Phys. Chem. Chem. Phys.*, 2005, **7**, 991–997.
40 E. E. Fileti and S. Canuto, Calculated Infrared Spectra of Hydrogen-Bonded Methanol–Water, Water–Methanol, and Methanol–Methanol Complexes, *Int. J. Quantum Chem.*, 2005, **104**, 808–815.
41 E. E. Fileti, M. A. Castro and S. Canuto, Calculations of vibrational frequencies, Raman activities and degrees of depolarization for complexes involving water, methanol and ethanol, *Chem. Phys. Lett.*, 2008, **452**, 54–58.
42 J. L. Iosue, D. M. Benoit and D. C. Clary, Diffusion Monte Carlo simulations of methanol–water clusters, *Chem. Phys. Lett.*, 1999, **301**, 275–280.
43 A. Galano, M. Narciso-Lopez and M. Francisco-Marquez, Water Complexes of Important Air Pollutants: Geometries, Complexation Energies, Concentrations, Infrared Spectra, and Intrinsic Reactivity, *J. Phys. Chem. A*, 2010, **114**, 5796–5809.
44 R. K. Campen and J. D. Kubicki, Interaction Energy and the Shift in OH Stretch Frequency on Hydrogen Bonding for the $H_2O \rightarrow H_2O$, $CH_3OH \rightarrow H_2O$ and $H_2O \rightarrow CH_3OH$ dimers, *J. Comput. Chem.*, 2009, **31**, 963–972.
45 D. González-Salgado and I. Nezbeda, Excess properties of aqueous mixtures of methanol: Simulation *versus* experiment, *Fluid Phase Equilib.*, 2006, **240**, 161–166.
46 B. G. Oliveira and M. L. A. A. Vasconcellos, Hydrogen bonds in alcohols:water complexes: A theoretical study about new intramolecular interactions *via* CHELPG and AIM calculations, *THEOCHEM*, 2006, **774**, 83–88.
47 D. Peeters and G. Leroy, Small clusters between water and alcohols, *THEOCHEM*, 1994, **314**, 39–47.
48 Y. Katrib, Ph. Mirabel, S. Le Calvé, G. Weck and E. Kochanski, Experimental Uptake Study of Ethanol by Water Droplets and Its Theoretical Modeling of Cluster Formation at the Interface, *J. Phys. Chem. B*, 2002, **106**, 7237–7245.
49 M. J. Frisch, G. W. Trucks, H. B. Schlegel, G. E. Scuseria, M. A. Robb, J. R. Cheeseman, J. A. Montgomery Jr., T. Vreven, K. N. Kudin, J. C. Burant, J. M. Millam, S. S. Iyengar, J. Tomasi, V. Barone, B. Mennucci, M. Cossi, G. Scalmani, N. Rega, G. A. Petersson, H. Nakatsuji, M. Hada, M. Ehara, K. Toyota, R. Fukuda, J. Hasegawa, M. Ishida, T. Nakajima, Y. Honda, O. Kitao, H. Nakai, M. Klene, X. Li, J. E. Knox, H. P. Hratchian, J. B. Cross, C. Adamo, J. Jaramillo, R. Gomperts, R. E. Stratmann, O. Yazyev, A. J. Austin, R. Cammi, C. Pomelli, J. W. Ochterski, P. Y. Ayala, K. Morokuma, G. A. Voth, P. Salvador, J. J. Dannenberg, V. G. Zakrzewski, S. Dapprich, A. D. Daniels, M. C. Strain, O. Farkas, D. K. Malick, A. D. Rabuck, K. Raghavachari, J. B. Foresman, J. V. Ortiz, Q. Cui, A. G. Baboul, S. Clifford, J. Cioslowski, B. B. Stefanov, G. Liu, A. Liashenko, P. Piskorz, I. Komaromi, R. L. Martin, D. J. Fox, T. Keith, M. A. Al-Laham, C. Y. Peng, A. Nanayakkara, M. Challacombe, P. M. W. Gill, B. Johnson, W. Chen, M. W. Wong, C. Gonzalez and J. A. Pople, *Gaussian 03, Revisions B.04 and C.02*, Gaussian Inc., Pittsburgh PA, 2003.
50 E. A. Gardner, A. Nevarez, M. Garbalena and W. C. Herndon, Infrared spectra and conformational analysis of anti and gauche deuterated ethanol isotopomers, *J. Mol. Struct.*, 2006, **784**, 249–253.
51 M. Albrecht, A. Borba, K. Le Barbu-Debus, B. Dittrich, R. Fausto, S. Grimme, A. Mahjoub, M. Nedić, U. Schmitt, L. Schrader, M. A. Suhm, A. Zehnacker-Rentien and J. Zischang, Chirality influence on the aggregation of methyl mandelate, *New J. Chem.*, 2010, **34**, 1266–1285.
52 R. M. Badger and S. H. Bauer, Spectroscopic studies of the hydrogen bond. II. The shift of the O–H vibrational frequency in the formation of the hydrogen bond, *J. Chem. Phys.*, 1937, **5**, 839–851.
53 M. Rozenberg, A. Loewenschuss and Y. Marcus, An empirical correlation between stretching vibration redshift and hydrogen bond length, *Phys. Chem. Chem. Phys.*, 2000, **2**, 2699–2702.
54 N. Bakkas, Y. Bouteiller, A. Louteiller, J. P. Perchard and S. Racine, The water–methanol complexes. Matrix induced structural conversion of the 1–1 species, *Chem. Phys. Lett.*, 1995, **232**, 90–98.
55 D. Peeters and P. Huyskens, Endothermicity or exothermicity of water/alcohol mixtures, *J. Mol. Struct.*, 1993, **300**, 539–550.
56 N. Bakkas, Y. Bouteiller, A. Louteiller, J. P. Perchard and S. Racine, The water–methanol complexes. I. A matrix isolation study and an *ab initio* calculation on the 1–1 species, *J. Chem. Phys.*, 1993, **99**, 3335–3342.
57 A. Zehnacker and M. A. Suhm, Chirality Recognition between Neutral Molecules in the Gas Phase, *Angew. Chem., Int. Ed.*, 2008, **47**, 6970–6992.
58 L. Evangelisti and W. Caminati, Internal dynamics in complexes of water with organic molecules. Details of the internal motions in *tert*-butylalcohol–water, *Phys. Chem. Chem. Phys.*, 2010, **12**, 14433–14441.
59 C. Leforestier, R. van Harrevelt and A. van der Avoird, Vibration–Rotation–Tunneling Levels of the Water Dimer from an *ab initio* Potential Surface with Flexible Monomers, *J. Phys. Chem. A*, 2009, **113**, 12285–12294.
60 G. Brink and L. Glasser, Studies in Hydrogen Bonding: Association within Small Clusters of Water, Methanol, and Ammonia Molecules Using Jorgensen's Intermolecular Pair Potentials, *J. Comput. Chem.*, 1982, **3**, 219–226.

61 J. R. Reimers and R. O. Watts, The structure and vibrational spectra of small clusters of water molecules, *Chem. Phys.*, 1984, **85**, 83–112.
62 O. Mó and M. Yáñez, Cooperative (nonpairwise) effects in water trimers: An *ab initio* molecular orbital study, *J. Chem. Phys.*, 1992, **97**, 6628–6638.
63 S. S. Xantheas and T. H. Dunning Jr., The structure of the water trimer from *ab initio* calculations, *J. Chem. Phys.*, 1993, **98**, 8037–8040.
64 J. K. Gregory and D. C. Clary, Structure of Water Clusters. The Contribution of Many-Body Forces, Monomer Relaxation, and Vibrational Zero-Point Energy, *J. Phys. Chem.*, 1996, **100**, 18014–18022.
65 W. O. George, B. F. Jones, R. Lewis and J. M. Price, Computer Modelling of Properties of Alcohols, *Internet J. Vib. Spec.*, 1999, **3**, 2–5.
66 W. O. George, B. F. Jones and R. Lewis, Water and its homologues: a comparison of hydrogen-bonding phenomena, *Philos. Trans. R. Soc. London, Ser. A*, 2001, **359**, 1611–1629.
67 U. Buck and F. Huisken, Infrared Spectroscopy of Size-Selected Water and Methanol Clusters, *Chem. Rev.*, 2000, **100**, 3863–3890.
68 G. Herzberg, *Molecular Spectra and Molecular Structure. II. Infrared and Raman Spectra of Polyatomic Molecules*, D. van Nostrand, 1945.
69 A. J. Easteal and L. A. Woolf, (p,V_m,Tx) measurements for $\{(1-x)H_2O + xCH_3OH\}$ in the range 278 to 323 K and 0.1 to 280 MPa, *J. Chem. Thermodyn.*, 1985, **17**, 69–82.
70 S. Burikov, S. Dolenko, T. Dolenko, S. Patsaeva and V. Yuzhakov, Decomposition of water Raman stretching band with a combination of optimization methods, *Mol. Phys.*, 2010, **108**, 739–747.
71 G. Graziano, Hydration thermodynamics of aliphatic alcohols, *Phys. Chem. Chem. Phys.*, 1999, **1**, 3567–3576.
72 T. Scharge, T. N. Wassermann and M. A. Suhm, Weak hydrogen bonds make a difference: Dimers of jet-cooled halogenated ethanols, *Z. Phys. Chem.*, 2008, **222**, 1407–1452.
73 R. Karaminkov, S. Chervenkov and H. J. Neusser, Water binding sites in 2-*para*- and 2-*ortho*-fluorophenylethanol: A high-resolution UV experiment and *ab initio* calculations, *J. Chem. Phys.*, 2010, **133**, 194301.
74 S. Tanimura, U. M. Dieregsweiler and B. E. Wyslouzil, Binary nucleation rates for ethanol/water mixtures in supersonic Laval nozzles, *J. Chem. Phys.*, 2010, **133**, 174305.
75 D. Nesbitt, T. Häber and M. A. Suhm, On the spectroscopy of argon-coated water and deuterium oxide clusters, *Faraday Discuss.*, 2001, **118**, 305–309.